



Geophysical Research Letters

RESEARCH LETTER

10.1029/2020GL090568

Key Points:

- For the first time, the Chandler wobble has been detected for a solar system body other than the Earth
- The Chandler wobble is visible in the tracking data from two Mars orbiting spacecraft
- The Chandler wobble significantly improves our understanding of the long period behavior of the mantle rheology

Supporting Information:

- Supporting Information S1

Correspondence to:

A. S. Konopliv,
alex.konopliv@jpl.nasa.gov

Citation:

Konopliv, A. S., Park, R. S., Rivoldini, A., Baland, R.-M., Le Maistre, S., Van Hoolst, T., et al. (2020). Detection of the Chandler wobble of Mars from orbiting spacecraft. *Geophysical Research Letters*, 47, e2020GL090568. <https://doi.org/10.1029/2020GL090568>

Received 31 AUG 2020

Accepted 9 OCT 2020

Accepted article online 13 OCT 2020

Detection of the Chandler Wobble of Mars From Orbiting Spacecraft

Alex S. Konopliv¹ , Ryan S. Park¹ , Attilio Rivoldini² , Rose-Marie Baland² , Sébastien Le Maistre² , Tim Van Hoolst² , Marie Yseboodt² , and Véronique Dehant²

¹Jet Propulsion Laboratory, California Institute of Technology, Pasadena, CA, USA, ²Royal Observatory of Belgium, Brussels, Belgium

Abstract For the first time for any planetary body other than the Earth, the free wobble of the pole called the Chandler wobble has been detected for Mars with a period of 206.9 ± 0.5 days and amplitude of 10 cm from radio tracking observations of Mars Odyssey, Mars Reconnaissance Orbiter (MRO), and Mars Global Surveyor (MGS), in order of decreasing sensitivity. The motion of the rotation pole location on the surface of Mars, or polar motion, is observed using two different approaches: (1) joint global estimates of Mars' orientation and its gravity field and (2) time series solutions of C_{21} and S_{21} . For Mars interior models, the Chandler wobble period is combined with other measurements including the moments of inertia from our estimated precession rate $\dot{\psi} = -7603.9 \pm 1.3$ mas/year and tidal Love number $k_2 = 0.169 \pm 0.006$. The Chandler wobble period constrains the rheology of the Martian mantle and in particular its long-term frequency dependence.

Plain Language Summary For the first time for any solar system body other than the Earth, one component of the motion of the Mars spin axis on the surface of Mars, called the Chandler wobble, has been detected. The motion has a period of 206.9 ± 0.5 days, an amplitude of 10 cm on the surface, and is in a nearly circular counterclockwise direction as viewed from the North Pole. The pole motion is determined from radio tracking observations of Mars Odyssey, Mars Reconnaissance Orbiter, and Mars Global Surveyor, in order of decreasing sensitivity. The detection of the Chandler wobble improves our understanding of energy dissipation in the mantle for time intervals near the wobble period.

1. Introduction

The path of the mean rotational pole relative to the surface of the body is referred to as polar motion and contains multiple components. The free mode due to the torque-free rotational equations of motion is called the free wobble or Chandler wobble (CW). If the pole is excited, it can be observed in polar motion, which has been known and measured for the Earth for over 100 years (e.g., Gross, 2015; Moritz & Mueller, 1988; Wahr, 1988). The Earth's polar motion is mostly a combination of the CW (3- to 6-m variable amplitude) with a period of 14 months and annual 12-month forced polar motion (3 m), resulting from seasonal atmospheric pressure changes (Merriam, 1982; Wahr, 1983). The CW path of the pole for the Earth and that expected for Mars on the surface is nearly circular counterclockwise motion (i.e., prograde) when viewed from above the North Pole.

Until now, polar motion has not been detected for any other solar system body, in part due to their slow rotation and less flattening (e.g., the Venus CW period is $\sim 10^5$ years; Yoder & Ward, 1979) or limited excitation and quick damping (Vesta and Ceres; Bills & Nimmo, 2011; Rambaux et al., 2011). The detection here is the CW component only, since its frequency is independent of the periods associated with the seasonal mass exchange between the polar ice caps. Indeed, the polar motion estimates from spacecraft tracking data of the Mars annual (1.881 year), semiannual, and other integral multiple terms are a mixture of forced polar motion and time-varying gravity coefficients from the ice-cap mass exchange. The contribution from the forced polar motion at these frequencies cannot be separated from the seasonal mass exchange component, since they both produce the same signature in the radio Doppler data. The amplitude of the CW for Mars is about 10 cm (or 6.1 mas) and significantly less than the Earth's amplitude. It is comparable in size to predicted forced polar motion amplitudes (10 mas annual, 15 mas semiannual; Van den Acker et al., 2002; Yoder & Standish, 1997), but much smaller than a plausible free wobble maximum value of 50 mas

(Yoder & Standish, 1997). Using estimation of the noise level in the angular momentum of the atmosphere of Mars, Dehant et al. (2006) have estimated the amplitude for different quality factor (Q) of the Martian mantle and have obtained amplitudes between 10 cm and 1.1 m, for Q between 80 and 200. Our observation is at the lower extreme of these estimations. Due to the small amplitude, the CW has been difficult to detect for Mars, with previous attempts unable to separate the Chandler frequency from the 1/3-Mars year seasonal mass term (Konopliv et al., 2006). However, with an additional 15 years of Mars Odyssey and MRO tracking data since then, the detection of the Mars CW has now become very clear. Solutions for the wobble period from all three spacecraft investigated (Mars Odyssey, MRO, and MGS) show consistent results near the combined solution of 206.9 ± 0.5 days, and solutions are not sensitive to various possible spacecraft force modeling errors.

The measured geodesy parameters that provide constraints for models of the Mars interior structure include the normalized polar moment of inertia C/MR_a^2 , which is derived from Mars' precession, and the solar tidal deformation as given by the Love number k_2 . Previously, it was shown that the measured k_2 indicates a liquid core inside Mars (Yoder et al., 2003), and together with the polar moment, it was used to constrain core size and density (e.g., Khan et al., 2018; Konopliv et al., 2011; Rivoldini et al., 2011; Zharkov & Gudkova, 2009).

The CW period is another constraint on the interior of Mars. It provides a measure of its capacity to deform at long periods significantly longer than tides, and its value is determined mainly by the mantle temperature, rheology, and composition. Predictions for the Mars CW period include 203.8 to 204.8 days (Zharkov & Gudkova, 2009) and 201 to 208 days (Van Hoolst et al., 2000). The modeled CW period P_{CW}^{rigid} for the case of a rigid body is given by the principal moments of inertia (equatorial moments A , B , and polar moment C):

$$P_{CW}^{rigid} = \frac{2\pi}{\omega} \left(\frac{AB}{(C-A)(C-B)} \right)^{\frac{1}{2}} \quad (1)$$

where ω is the body spin rate. $P_{CW}^{rigid} = 191.5$ days for a triaxial Mars, and the period is 1 day longer versus a two-axial or rotationally symmetric Mars ($A = B$) (Zharkov & Gudkova, 2009). The rigid-body period is significantly less than the observed value of 206.9 days. For Earth, the rigid-body prediction is 305 days, and the observed Chandler period is 433.0 ± 1.1 days (Gross, 2015), an even larger increase due to a larger Love number k_2 (mostly due to the Earth being elastic and more massive than Mars) and a smaller secular Love number k_0 (also called fluid Love number) that enters in the denominator in the expression of the Chandler period. The modeled CW period P_{CW} for a triaxial elastic body with a liquid core is given by (e.g., Zharkov & Gudkova, 2009, equation 8)

$$P_{CW} = \frac{P_{CW}^{rigid} \left(1 - \left(\frac{A_c B_c}{AB} \right)^{\frac{1}{2}} \right)}{\left(1 - \frac{k_2}{k_0} \right)} \quad (2)$$

where A_c and B_c are the equatorial moments of the core, $k_0 = \frac{3(C-A)G}{\omega^2 R_a^5} = \frac{3J_2 g}{\omega^2 R_a^5}$, g the surface acceleration, J_2 the oblateness coefficient, and R_a the average radius of Mars. For the rotationally symmetric case, the moment of inertia term simplifies to (A_m/A) , where A_m is the equatorial moment of the mantle.

Mars' CW will damp out quickly (~60 years; Yoder & Standish, 1997) unless there is an excitation, which for Earth is mostly thought to be related to atmospheric, oceanic, and hydrologic processes (Gross, 2000, 2015). For Mars, the excitation is related to the seasonal mass exchange between the Mars polar caps, and mostly driven by atmospheric pressure changes especially near the one-third Mars year frequency (Yoder & Standish, 1997), which is close to the Chandler frequency.

2. Method of Polar Motion Detection

The polar motion of Mars is detected from the dynamical effect it has on the orbit of the Mars spacecraft. The orbit is determined from X-band Doppler tracking of the spacecraft with a typical measurement

accuracy for 10-s samples between ~0.03–0.07 mm/s of the velocity in the line-of-sight direction from Earth to Mars depending on the Sun angle (e.g., see Figure 2 in Konopliv et al., 2011). In order to better constrain the orientation of Mars, lander data from Mars Pathfinder, Viking landers, and Mars Exploration Rover (MER) Opportunity tracking data are also included (see Table S1 in the supporting information). The orbiter tracking data for MRO (Zuber et al., 2007) and MGS (Tyler et al., 1992) were collected and archived as part of radio science investigations, whereas Mars Odyssey was archived without a radio science experiment.

The polar motion of Mars is estimated using two different approaches. The first method is to globally estimate the polar motion together with the gravity field of Mars and other orientation parameters (Folkner et al., 1997; Konopliv et al., 2006) using the three orbiters and four landers. The method is the same as used for the previous Mars gravity determination (MRO120D; Konopliv et al., 2016) except for the additional estimation of polar motion amplitudes (annual, semiannual, one-third annual, one-fourth annual, and CW) and CW period. Also, an additional 4 years of orbiter tracking data are included to produce the new gravity field named MRO120F.

The second method determines the polar motion by generating a time series of solutions from local or arc-dependent estimates of the C_{21} and S_{21} gravity coefficients from each data arc (~4 days) using the newly derived MRO120F gravity field (minus polar motion parameters). Only the local parameters (spacecraft state, atmospheric drag, and spacecraft thrusting, which are determined independently for each data arc) are estimated together with C_{21} , S_{21} , and J_3 . All other parameters (orientation and gravity) are held fixed to MRO120F values. The estimated gravity terms are actually linear combinations of other same order coefficients where the odd zonal coefficients (represented by J_3) are the best determined (Konopliv et al., 2006). However, the even zonal coefficients are not as well known, and the predicted contributions from the NASA Ames Mars global circulation model (Haberle et al., 1999, 2008) are used to avoid any biasing in the polar motion solution. The polar motion is then given by the spectral analysis of all the arc-by-arc solutions for C_{21} and S_{21} using a Lomb-Scargle periodogram. This second method has the benefit to show the signal for all frequencies and note any other frequency dependence than those estimated in the global solution. The second method also determines the CW period independently for each gravity coefficient, but since they should be equal, it is a measure of the robustness of the wobble period estimate.

The estimation of the polar motion angles through the rotation matrices (Folkner et al., 1997) is equivalent to the estimation of polar motion using C_{21} and S_{21} gravity coefficients. The degree 2 gravity coefficients are related to the moments of inertia (e.g., Lambeck, 1988, equation 2.2.2), and the directions of the principal axes are given by the eigenvectors from diagonalizing the inertia matrix. The polar motion angles (X_p , Y_p) of the spin pole relative to the polar principal axis or body-fixed frame as defined by Folkner et al. (1997) are given by (e.g., Marchenko & Schwintzer, 2003, equation 91)

$$X_p = -\frac{(\sqrt{3J_2} - \bar{C}_{22})\delta\bar{C}_{21} - \bar{S}_{22}\delta\bar{S}_{21}}{(3\bar{J}_2^2 - \bar{C}_{22}^2 - \bar{S}_{22}^2)}, \quad Y_p = \frac{(\sqrt{3J_2} + \bar{C}_{22})\delta\bar{S}_{21} - \bar{S}_{22}\delta\bar{C}_{21}}{(3\bar{J}_2^2 - \bar{C}_{22}^2 - \bar{S}_{22}^2)} \quad (3)$$

where the degree 2 coefficients are normalized (Kaula, 1966) and $\delta\bar{C}_{21}$ and $\delta\bar{S}_{21}$ represent changes relative to the mean. Since J_2 of Mars is large, the error in neglecting S_{22} in the numerator only is about 3% for the amplitudes and the time history of X_p is given by δC_{21} and Y_p is given by δS_{21} .

The time-varying changes in the C_{21} and S_{21} gravity field (and hence polar motion) are mostly determined from longer period or m-daily (~24 hr or thus longer than the ~2 hr orbit period) changes in the spacecraft orbit longitude of ascending node Ω with respect to the Mars equator (Konopliv et al., 2006, equation 3). Because of the nearly polar spacecraft orbits, there are no other significant secular or long-period changes due to C_{21} and S_{21} for the other classical elements (they are $\cos i = 0.05$ smaller). Each order 1 coefficient contributes to the amplitude of the long period term so that the observed amplitude is a combination of even degree order 1 coefficients that to first order are not separable (any separation comes from much smaller short period terms driven by the orbit period). Attempts to additionally estimate C_{41} and S_{41} increase C_{21} and S_{21} uncertainties by ~10 times and solution correlations are ~0.99 between the degrees 2 and 4 coefficients. For a polar orbit, the observed seasonal gravity is given by the combination of unnormalized

coefficient amplitudes $\delta C_{21}(obs) \equiv \delta C_{21} + 1.52\delta C_{41} + 1.79\delta C_{61} + 1.89\delta C_{81} + \dots$ (with the same expression for S_{21}). Since C_{21} and S_{21} are determined by the orbital node changes, the best coefficient estimates come from orbit geometries that are near face-on when viewed from Earth (see Figure 12 of Konopliv et al., 2006).

3. Polar Motion and Other Estimates

The global solution of the polar motion is estimated as a series in Mars mean anomaly M plus the CW term as given by

$$\begin{aligned} X_p(t) &= \sum_{j=1}^5 (X_{cj} \cos m(j) + X_{sj} \sin m(j)) \\ Y_p(t) &= \sum_{j=1}^5 (Y_{cj} \cos m(j) + Y_{sj} \sin m(j)) \end{aligned} \quad (4)$$

where $m(j) = j^*M$ for $j = 1$ to 4 and $m(j) = 3.3188^*M$ for $j = 5$. In addition to the amplitudes, the frequency of the last term is estimated as a CW period (nominally 207 days; i.e., $3.3188 = 687/207$). The polar motion is estimated together with Mars spin pole location at epoch, precession, obliquity rate, rotational spin rate, Mars seasonal spin (ΔLOD), Mars and Phobos and Deimos GM , k_2 Love number (as determined by k_{22}), a 120th degree spherical harmonic gravity field, seasonal changes in the J_3 gravity coefficient, and spacecraft bus and solar array reflectivity parameters (see Table S2 for Mars orientation estimates). The parameters estimated are nearly identical to previous Mars gravity field estimates (Konopliv et al., 2016) but additionally include polar motion.

The global solutions for the polar motion in Equation 4 for all data and solutions using only each spacecraft (Odyssey, MRO, and MGS) are given in Figure 1 (Table S3). Again, solutions that are multiples of the Mars annual frequency are a combination of forced polar motion and seasonal changes in the Mars gravity coefficients. However, the observed annual term is mostly a combination of seasonal mass changes from C_{41} , C_{61} , and so forth since the seasonal mass C_{21} term mostly cancels the forced polar motion (Konopliv et al., 2006, equation 31). The CW has an amplitude of ~ 7 mas (10 cm on the surface) and shows consistent near circular counterclockwise motion for all data sets (Figure 1). The CW period estimate for all data in MRO120F is $P_{CW} = 206.9 \pm 0.5$ days. The uncertainty in the wobble period is realistic (see Konopliv et al., 2016), where the uncertainty in the orientation parameters and low degree gravity field are increased by about a factor of 10 over the formal uncertainty. The wobble period solution is very robust and shows minimal correlation with other parameters such as seasonal spin ($\rho < 0.05$), Love number ($\rho < 0.05$), precession spin ($\rho < 0.01$), and spacecraft solar pressure ($\rho < 0.005$) but shows some dependence on one third per year ($\rho \sim 0.1$) and CW amplitudes ($\rho \sim 0.3$). The wobble solution was also tested for different a priori values versus the nominal a priori of 207.0 ± 10 days. An a priori value of 208 days increased the solution by 0.1 day, and larger a priori values further away from the nominal (205 and 212 days) shifted significantly toward 207 days but requires multiple iterations to converge. We also note that the second arc-by-arc approach is independent of an a priori value and uncertainty.

The second approach determines the CW from estimates of C_{21} and S_{21} for each data arc of about 4 days in length. Since one can see the individual arc-by-arc contributions (as opposed to the global method which groups all arcs together), this method allows for easier removal of outlier solutions for the gravity coefficients and poorly determined estimates based upon the solution uncertainty. Figure 2 shows the resulting periodogram for the Mars Odyssey arc-by-arc solutions. The amplitudes from the seasonal cap mass exchange and forced polar motion are evident, with no other frequencies noted in the spectrum other than the CW. The CW now becomes very clear with the additional 15 years of data and is easily separated from the one-third Mars year seasonal term, which was not the possible previously (Konopliv et al., 2006). The independently determined wobble periods from C_{21} (206.73 days) and S_{21} (206.68 days) match well within the global uncertainty of 0.5 days and agree well with the global estimate of 206.9 days. The same analysis was done for the MRO and MGS spacecraft (Figure S1), and both validate the Mars Odyssey results, but with less accuracy, likely due to atmospheric drag for MRO and less data for MGS. Again, the independently determined wobble periods from C_{21} and S_{21} match fairly well for MRO (207.81 and 207.34 days) and

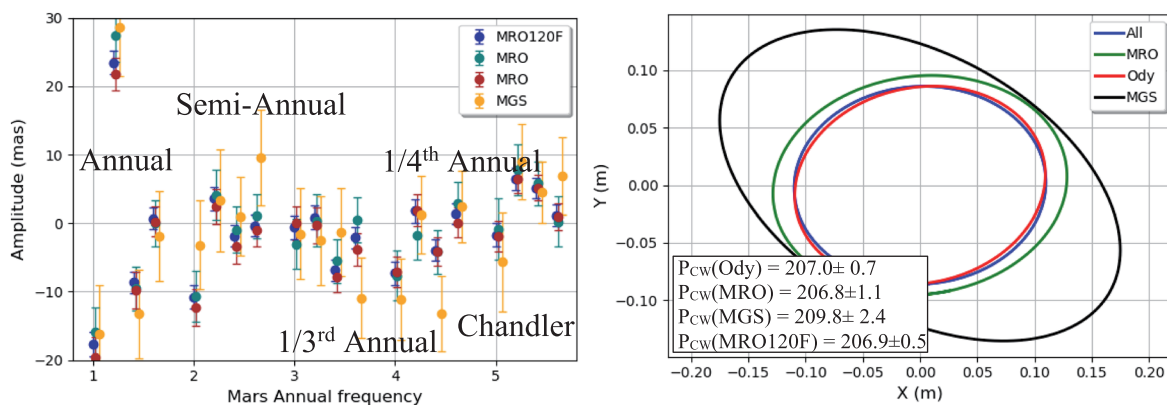


Figure 1. Global solution for polar motion amplitude (left) and the Chandler wobble component motion of the spin pole on the surface of Mars as viewed from above the North Pole (right). The left x axis ($x = 1, 2, 3, 4, 5$) represents Mars annual, semiannual, one-third annual, one-fourth annual, and CW solutions as given by Equation 4, respectively. The order of the amplitudes is X cosine and sine and then Y cosine and sine.

MGS (207.86 and 208.62 days), and the differences with the global solution are within uncertainties for MRO of 1.1 days and MGS of 2.4 days.

The other parameter estimates of interest for Mars interior modeling (see Table S4) are the precession rate $\dot{\psi}_o$ and tidal Love number k_2 . While the solution for the CW period is very stable with limited correlation with other parameters, the solution for $\dot{\psi}$ and k_2 are more strongly correlated with other parameters. The

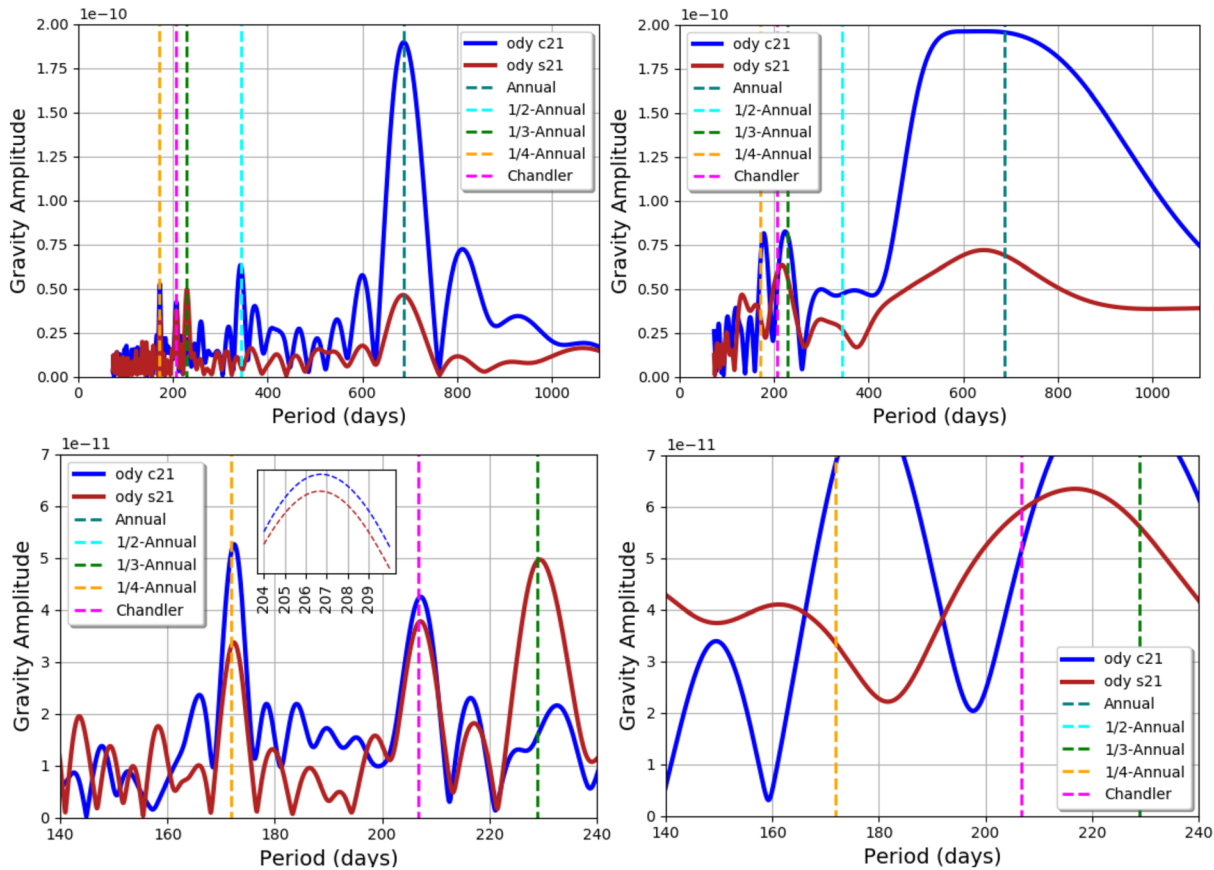


Figure 2. Mars polar motion periodogram from arc-by-arc solutions of C_{21} and S_{21} from Mars Odyssey. The left column shows the solution for the full 18 years of tracking data. The right column shows the solution with the same time span used in the previous attempt (Konopliv et al., 2006), which has an end time of March 2005. The bottom row shows an enlargement with an inset for the CW.

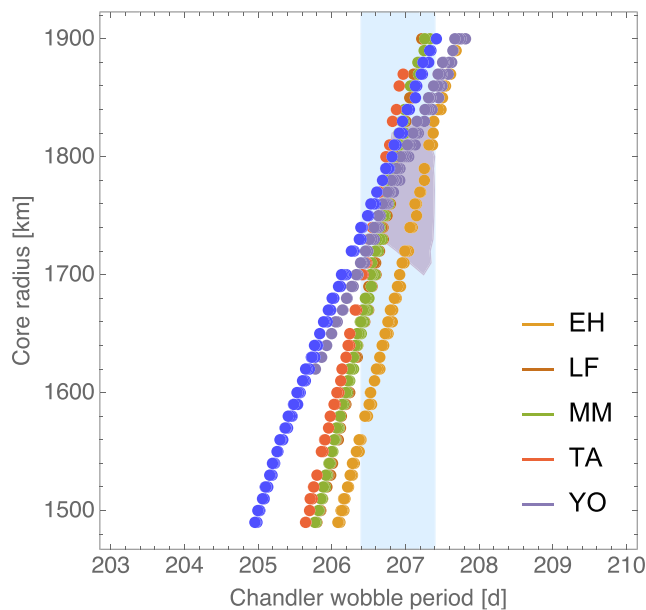


Figure 3. Core radius as function of Chandler wobble period for Mars mantle models of Sanloup et al. (1999) (EH), Lodders and Fegley (1997) (LF), Mohapatra and Murty (2003) (MM), Taylor (2013) (TA), and Yoshizaki and McDonough (2020) (YO). For all models the hot end-member temperature profile of Plesa et al. (2016) (Case 16) has been used. To illustrate the effect of mantle temperature, the Yoshizaki model is also shown for the cold end-member (Case 22 from Plesa et al., 2016) temperature profile (darker blue dots). The lighter blue shaded area represents the CW period of this study at 1σ . The purplish area represents YO mantle models with the hot end-member temperature that agree with the CW period, semidiurnal tidal Love number k_{22} , and secular acceleration of Phobos at 1σ . The surface area results from the variation of the rheology parameters α in the frequency-to-the-power- α dependence of the rheology due to anelasticity and ranges for Q_0 .

precession rate is correlated with the precession at initial epoch ψ_o ($\rho \sim 0.8$), epoch prime meridian ϕ_o ($\rho \sim 0.2$), spin rate $\dot{\phi}_o$ ($\rho \sim 0.6$), seasonal spin ($\rho \sim 0.1$), core factor for nutation F ($\rho \sim 0.2$) and period σ_o ($\rho \sim 0.05$), tidal Love number k_2 ($\rho \sim 0.1$), and spacecraft solar pressure ($\rho \sim 0.1$). The precession rate solution $\dot{\psi} = -7,603.9 \pm 1.3$ mas/year is globally determined (MRO120F) from all spacecraft data. Although not nominally estimated for MRO120F (Table S2), solution uncertainty in the liquid core amplification factor F is $\sim 30\%$ of the nominal value but will eventually be determined by InSight (Folkner et al., 2018; see Figure 1). The Love number strongly depends on the modeling of the spacecraft solar pressure for all spacecraft ($\rho \sim 0.3$) and some on the core factor F ($\rho \sim 0.2$) and period ($\rho \sim 0.2$), and precession ($\rho \sim 0.1$). The current solution for $k_2 = 0.169 \pm 0.006$ from MRO120F is identical with the previous solution (Konopliv et al., 2016). For our anelastic interior modeling, the observed k_2 is corrected for atmospheric tide (and not for anelastic softening) and normalized to the average radius. The atmospheric tidal correction used here was determined from Pathfinder pressure data (Konopliv et al., 2006). It increases k_2 by 0.003. More recent data from MSL or InSight indicate that the atmospheric tide correction to k_2 depends on the atmospheric conditions at the time of the observations. To take into account this supplementary uncertainty, we increase the uncertainty on k_2 by 0.002, resulting in $k_2 = 0.174 \pm 0.008$.

4. Mars Interior Modeling

The CW provides insight into Mars' interior since it essentially describes a rotational motion of the mantle only and is affected by the deformation of Mars in response to the variable centrifugal acceleration. As it is a free motion, the information on the interior is mainly contained in the period, not in its amplitude, which to a large extent reflects how Mars reacts rotationally to atmospheric forcing at the period band of the CW. The two main interior characteristics that the CW period, P_{CW} , depends upon are

the ratio of the total planet moment of inertia to that of the mantle, $\frac{A}{A_m}$, and the Love number k_2 at the Chandler period (see Equation 2). Deformation due to changes in the centrifugal acceleration associated with the wobble lengthens the CW period because it increases the inertia tensor. A larger core leads to a larger deformation, or larger k_2 , and therefore a larger CW period. It also implies that the moment of inertia of the mantle is smaller (or, if $\frac{A}{A_m}$ is larger) and therefore the CW period smaller. Although both $\frac{A}{A_m}$ and k_2 depend sensitively on the size of the core, their opposite effects on CW period nearly cancel so that the CW period itself only marginally depends on the core size (Van Hoolst et al., 2000). Another important property that affects the period of the CW is the rheology of the mantle. Anelastic behavior of the mantle decreases the mantle rigidity and therefore increases k_2 and the CW period. For the Earth the effect is significant since it extends the CW period of an elastic model with a liquid core and solid inner core (402 days; Smith, 1977) by about 97 days.

Figure 3 shows that the CW period for a set of models (Text S1) for different plausible Mars mantle compositions and two mantle temperature end-members that agree with the moment of inertia (MOI) of this study at 1σ . The core radius of MOI compatible models increases from about 1,500 km to about 1900 km whereas the CW period only increases by less than 4 days. If the core range is reduced to models that agree also with k_2 (1,750–1,880 km; see Figure S2), the P_{CW} range is reduced by about 1 day (Figure 3). The composition of the mantle affects the CW period only marginally. The almost parallel shift in the core radius range as a function of the CW period of all the mantle composition models, except Yoshizaki and McDonough, results from the different mantle moment of inertia and to a lesser extent from the differences in k_2 (see Figure S2) of those

models. The slope of the CW period–core radius relation increases faster for the Yoshizaki and McDonough models because k_2 increases faster with core radius (see Figure S2). This effect occurs mainly because the effective mantle rigidity of the Fe poorer model of Yoshizaki and McDonough decreases faster with core radius than that of the other models that have a larger but almost identical Fe content in the mantle. The mantle rigidity is also affected by the mantle temperature. The cold mantle temperature which is about 350 K colder at the core–mantle boundary than the hot end-member (Plesa et al., 2016, Cases 16 and 22) decreases the CW by about 1 day (see Figure 3). Taken together, mantle compositional and temperature effects induce a variation in the CW period that is about 1.5 days for a given core radius, that is, about 3 times the CW period uncertainty.

The results shown in Figure 3 represent the predicted CW periods of triaxial anelastic plausible Mars models. Triaxiality increases the wobble period by about 0.5 days versus biaxial and therefore has a small effect of the same order as the CW uncertainty. Anelasticity, on the other hand, is essential in explaining the observational value as it lengthens the CW period with respect to an elastic mantle by several days (see Figure S3). To model the rheology of the mantle, we assume a simple frequency-dependent and depth-independent shear dissipation (Text S1). The parameters that govern the shear dissipation, the frequency exponent α and the Q-factor normalization Q_o (Equation S1), are adjusted such that the predicted k_2 and the CW period agree with the results of this study as well as with the secular acceleration of Phobos (Lainey et al., 2007). Based on a gridded systematic parameter space exploration for each mantle model and by assuming a core radius of 1,790 km, we find that α can vary from 0.07 to 0.25 and Q_o from 78 to 90 for the models with the hot end-member temperature. Models with the cold temperature end-member models have a stiffer elastic mantle and require a softer rheology and a larger core to match observations. For the models that use the Yoshizaki and McDonough (2020) mantle composition with the cold temperature end-member, we assume a core radius of 1,840 km, α is between 0.29 and 0.35, and Q_o is between 78 and 79. The variation in the range of parameter values between different mantle composition models is small (see Table S6). The CW period determined in this study provides an important constraint on the frequency dependence α of the mantle rheology. The range of α values is significantly reduced if compared to the range provided by the anelastic k_2 Love number and secular acceleration measurements (see Table S6).

The range of α required to explain the CW period of the Earth is between 0.12 and 0.37 (Anderson & Minster, 1979, updated with Q_{CW} from Gross, 2015) is roughly comparable to that we have deduced for the Mars models with a 1,790 km core radius. We note that the Earth model is anchored at different periods than used for Mars: 54 min for the spheroidal seismic mode ${}_0S_2$ and 433 days for the period of the CW.

Because of the anelastic mantle, the CW would freely decay if it were not excited. Its decay time is characterized by the quality factor $Q_{CW} = \frac{Re(\tau_{CW})}{Im(\tau_{CW})}$. For the hot end-member Yoshizaki and McDonough (2020) model with a core radius of 1,790 km, Q_{CW} is between 98 and 322 and that associated to the cold temperature end-member with a core radius of 1,840 km is between 40 and 65 (see Figures S2 and S3, also for other mantle compositions).

The Q_{CW} range of the composition and thermal models of Mars considered here (40–350) overlaps with that estimated for the Earth, 74–789 (Gross, 2015), but the anelastic damping of the Martian mantle is significantly larger at the CW period. Therefore, the time it would take for the CW to freely decay if not excited is significantly shorter for Mars. The e-folding amplitude decay time, $\frac{2}{2\pi} Q_{CW} \tau_{CW}$, for Mars is between 7 and 63 years whereas for the Earth it is 28 to 299 years (at 1σ) (Gross, 2015). Like for the Earth, the CW decay time is relatively short on a geological time scale; thus, it must be excited by some mechanism. For Mars the principal excitation mechanism is likely of atmospheric origin (Dehant et al., 2006) whereas excitations produced by core–mantle interactions or marsquakes are unlikely but cannot be excluded (see Gross, 2015, for a discussion about CW excitation mechanism for Earth).

5. Conclusions

The Mars CW is clearly detected by both Mars Odyssey and MRO, where the best detection comes from the 18 years of data from Mars Odyssey. Previous attempts to see the wobble were unsuccessful due to the

limited amount of data at the time (Konopliv et al., 2006). The solution for the wobble is robust, and insensitive to possible systematic errors in spacecraft nongravitational force models. Because of its long period, knowledge of the CW significantly improves our understanding of the long period behavior of the mantle rheology. This information is complementary to data about the tidal Love number and nutation of Mars and improves their interpretation in terms of interior structure and core radius. The nutation terms, sensitive to the core size and shape as well as to the rheology of the mantle, are expected to be measured precisely by InSight.

Data Availability Statement

The data used in this study (including MRO120F) are available online from the PDS (at <https://pds-geosciences.wustl.edu/>).

Acknowledgments

The research was carried out at the Jet Propulsion Laboratory, California Institute of Technology, under a contract with the National Aeronautics and Space Administration (80NM0018D0004). The work of A. R., R. -M. B., S. L. M., T. V. H., M. Y., and V. D. was financially supported by the Belgian PRODEX program managed by the European Space Agency in collaboration with the Belgian Federal Science Policy Office. Also, A. K. would like to thank Chuck Yoder for his collaboration and insight on previous multiple attempts to detect the Chandler wobble, which formed the basis for this effort. We also acknowledge Bill Folkner's help in the previous processing of the lander tracking data used in this study.

References

- Anderson, D. L., & Minster, J. B. (1979). The frequency dependence of Q in the Earth and implications for mantle rheology and Chandler wobble. *Geophysical Journal of the Royal Astronomical Society*, 58(2), 431–440. <https://doi.org/10.1111/j.1365-246X.1979.tb01033.x>
- Bills, B. G., & Nimmo, F. (2011). Forced obliquities and moments of inertia of Ceres and Vesta. *Icarus*, 213(2), 496–509. <https://doi.org/10.1016/j.icarus.2010.09.002>
- Dehant, V., de Viron, O., Karatekin, O., & Van Hoolst, T. (2006). Excitation of Mars polar motion. *Astronomy and Astrophysics*, 446, 345–355. <https://doi.org/10.1051/0004-6361:20053825>
- Folkner, W. M., Dehant, V., LeMaistre, S., Yseboodt, M., Rivoldini, A., Van Hoolst, T., et al. (2018). The rotation and interior structure experiment on the InSight Mission to Mars. *Space Science Reviews*, 214, 100. <https://doi.org/10.1007/s11214-018-0530-5>
- Folkner, W. M., Kahn, R. D., Preston, R. A., Yoder, C. F., Standish, E. M., Williams, J. G., et al. (1997). Mars dynamics from Earth-based tracking of the Mars Pathfinder lander. *Journal of Geophysical Research*, 102(E2), 4057–4064. <https://doi.org/10.1029/96JE02125>
- Gross, R. (2000). The excitation of the Chandler wobble. *Geophysical Research Letters*, 27(15), 2329–2332. <https://doi.org/10.1029/2000GL011450>
- Gross, R. S. (2015). Earth rotation variations—Long period. In T. A. Herring (Ed.), *Physical Geodesy, Treatise on Geophysics* (Vol. 11, pp. 239–294). Amsterdam: Elsevier.
- Haberle, R. M., Forget, F., Colaprete, A., Schaeffer, J., Boynton, W. V., Kelly, N. J., & Chamberlain, M. A. (2008). The effect of ground ice on the Martian seasonal CO₂ cycle. *Planetary and Space Science*, 56(2), 251–255. <https://doi.org/10.1016/j.pss.2007.08.006>
- Haberle, R. M., Joshi, M. M., Murphy, J. R., Barnes, J. R., Schofield, J. T., Wilson, G., et al. (1999). General circulation model simulations of the Mars Pathfinder atmospheric structure investigation/meteorology data. *Journal of Geophysical Research*, 104(E4), 8957–8974. <https://doi.org/10.1029/1998JE900040>
- Kaula, W. M. (1966). *Theory of Satellite Geodesy*. Waltham, MA: Blaisdell.
- Khan, A., Liebske, C., Rozel, A., Rivoldini, A., Nimmo, F., Connolly, J. A. D., et al. (2018). A geophysical perspective on the bulk composition of Mars. *Journal of Geophysical Research: Planets*, 123, 575–611. <https://doi.org/10.1002/2017JE005371>
- Konopliv, A. S., Asmar, S. W., Folkner, W. M., Karatekin, O., Nunes, D. C., Smrekar, S. E., et al. (2011). Mars high resolution gravity fields from MRO, Mars seasonal gravity, and other dynamical parameters. *Icarus*, 211, 401–428. <https://doi.org/10.1016/j.icarus.2010.10.004>
- Konopliv, A. S., Park, R. S., & Folkner, W. M. (2016). An improved JPL Mars gravity field and orientation from Mars Orbiter and Lander tracking data. *Icarus*, 274, 253–260. <https://doi.org/10.1016/j.icarus.2016.02.052>
- Konopliv, A. S., Yoder, C. F., Standish, E. M., Yuan, D. N., & Sjogren, W. L. (2006). A global solution for the Mars static and seasonal gravity, Mars orientation, Phobos and Deimos masses, and Mars ephemeris. *Icarus*, 182, 23–50. <https://doi.org/10.1016/j.icarus.2005.12.025>
- Lainey, V., Dehant, V., & Pätzold, M. (2007). First numerical ephemerides of the two Martian moons. *Astronomy and Astrophysics*, 465(3), 1075–1084. <https://doi.org/10.1051/0004-6361:20065466>
- Lambeck, K. (1988). *Geophysical geodesy*. Oxford: Clarendon (Oxford University Press).
- Lodders, K., & Fegley, B. (1997). An oxygen isotope model for the composition of Mars. *Icarus*, 126, 373–394. <https://doi.org/10.1006/icar.1996.5653>
- Marchenko, A. N., & Schwintzer, P. (2003). Estimation of the Earth's tensor of inertia from recent global gravity field solutions. *Journal of Geodesy*, 76(9–10), 495–509. <https://doi.org/10.1007/s00190-002-0280-7>
- Merriam, J. (1982). Meteorological excitation of the annual polar motion. *Geophysical Journal of the Royal Astronomical Society*, 70(1), 41–56. <https://doi.org/10.1111/j.1365-246X.1982.tb06390.x>
- Mohapatra, R. K., & Murty, S. V. S. (2003). Precursors of Mars: Constraints from nitrogen and oxygen isotopic compositions of Martian meteorites. *Meteoritics and Planetary Science*, 38(2), 225–241. <https://doi.org/10.1111/j.1945-5100.2003.tb00261.x>
- Moritz, H., & Mueller, I. I. (1988). *Earth rotation: Theory and observation*. New York: The Ungar Publishing Co.
- Plesa, A. C., Grott, M., Tosi, N., Breuer, D., Spohn, T., & Wieczorek, M. A. (2016). How large are present-day heat flux variations across the surface of Mars? *Journal of Geophysical Research: Planets*, 121, 2386–2403. <https://doi.org/10.1002/2016JE005126>
- Rambaux, N., Castillo-Rogez, J., Dehant, V., & Kuchynka, P. (2011). Constraining Ceres' interior from its rotational motion. *Astronomy and Astrophysics*, 535, A43. <https://doi.org/10.1051/0004-6361/201116563>
- Rivoldini, A., Van Hoolst, T., Verhoeven, O., Mocquet, A., & Dehant, V. (2011). Geodesy constraints on the interior structure and composition of Mars. *Icarus*, 213, 451–472. <https://doi.org/10.1016/j.icarus.2011.03.024>
- Sanloup, C., Jambon, A., & Gillet, P. (1999). A simple chondritic model of Mars. *Physics of the Earth and Planetary Interiors*, 112(1–2), 43–54. [https://doi.org/10.1016/S0031-9201\(98\)00175-7](https://doi.org/10.1016/S0031-9201(98)00175-7)
- Smith, M. L. (1977). Wobble and nutation of the Earth. *Geophysical Journal of the Royal Astronomical Society*, 64(1), 223–281. <https://doi.org/10.1111/j.1365-246X.1981.tb02667.x>
- Taylor, G. J. (2013). The bulk composition of Mars. *Chemie der Erde*, 73, 401–420. <https://doi.org/10.1016/j.chemer.2013.09.006>

- Tyler, G. L., Balmino, G., Hinson, D. P., Sjogren, W. L., Smith, D. E., Woo, R., et al. (1992). Radio science investigations with Mars Observer. *Journal of Geophysical Research*, 97(E5), 7759–7779. <https://doi.org/10.1029/92JE00513>
- Van den Acker, E., Van Hoolst, T., de Viron, O., Defrainge, P., Forget, F., Hourdin, F., & Dehant, V. (2002). Influence of winds and the CO₂ mass exchange between the atmosphere and the polar caps on Mars rotation. *Journal of Geophysical Research*, 107(E7), 5055. <https://doi.org/10.1029/2000JE001539>
- Van Hoolst, T., Dehant, T., & Defraigne, P. (2000). Chandler wobble and free core nutation for Mars. *Planetary and Space Science*, 48(12–14), 1145–1151. [https://doi.org/10.1016/S0032-0633\(00\)0099-4](https://doi.org/10.1016/S0032-0633(00)0099-4)
- Wahr, J. (1983). The effects of the atmosphere and oceans on the Earth's wobble and on the seasonal variations in the length of day—II. Results. *Geophysical Journal of the Royal Astronomical Society*, 74, 451–487.
- Wahr, J. M. (1988). The Earth's rotation. *Annual Review of Earth and Planetary Sciences*, 16(1), 231–249. <https://doi.org/10.1146/annurev.ea.16.050188.001311>
- Yoder, C. F., Konopliv, A. S., Yuan, D. Y., Standish, E. M., & Folkner, W. M. (2003). Fluid core size of Mars from detection of the solar tide. *Science*, 300(5617), 299–303. <https://doi.org/10.1126/science.1079645>
- Yoder, C. F., & Standish, E. M. (1997). Martian precession and rotation from Viking lander range data. *Journal of Geophysical Research*, 102(E2), 4065–4080. <https://doi.org/10.1029/96JE03642>
- Yoder, C. F., & Ward, W. R. (1979). Does Venus wobble? *The Astrophysical Journal*, 233, L33–L37. <https://doi.org/10.1086/183071>
- Yoshizaki, T., & McDonough, W. F. (2020). The composition of Mars. *Earth and Planetary Astrophysics*, 273, 137–162. <https://doi.org/10.1016/j.gca.2020.01.11>
- Zharkov, V., & Gudkova, T. (2009). The period and Q of the Chandler wobble of Mars. *Planetary and Space Science*, 57, 288–295. <https://doi.org/10.1016/j.pss.2008.11.010>
- Zuber, M. T., Lemoine, F. G., Smith, D. E., Konopliv, A. S., Smrekar, S. E., & Asmar, S. W. (2007). Mars Reconnaissance Orbiter radio science investigation. *Journal of Geophysical Research*, 112, E05S07. <https://doi.org/10.1029/2006JE002833>

References From the Supporting Information

- Connolly, J. A. D. (2005). Computation of phase equilibria by linear programming: A tool for geodynamic modeling and its application to subduction zone decarbonation. *Earth and Planetary Science Letters*, 236(1–2), 524–541. <https://doi.org/10.1016/j.epsl.2005.04.033>
- Kaula, W. M. (1964). Tidal dissipation by solid friction and the resulting orbital evolution. *Reviews of Geophysics*, 2(4), 661–685. <https://doi.org/10.1029/RG002i004p00661>
- Pätzold, M., Andert, T., Jacobson, R., Rosenblatt, P., & Dehant, V. (2014). Phobos: Observed bulk properties. *Planetary and Space Science*, 102, 86–94. <https://doi.org/10.1016/j.pss.2014.01.004>
- Stixrude, L., & Lithgow-Bertelloni, C. (2011). Thermodynamics of mantle minerals—II. Phase equilibria. *Geophysical Journal International*, 184(3), 1180–1213. <https://doi.org/10.1111/j.1365-246X.2010.04890.x>
- Terasaki, H., Rivoldini, A., Shimoyama, Y., Nishida, K., Urakawa, S., Maki, M., et al. (2019). Pressure and composition effects on sound velocity and density of core-forming liquids: Implication to core compositions of terrestrial planets. *Journal of Geophysical Research: Planets*, 124, 2272–2293. <https://doi.org/10.1029/2019JE005936>
- Wieczorek, M. A., & Zuber, M. T. (2004). Thickness of the Martian crust: Improved constraints from geoid-to-topography ratios. *Journal of Geophysical Research*, 109, E01009. <https://doi.org/10.1029/2003JE002153>